We A1 01

Numerical Assessment Of Water Alternating Gas Practices In The Presence Of Hysteresis Effects On Relative Permeability

E. Ranaee* (Politecnico Di Milano), F. Inzoli (Politecnico Di Milano), M. Riva (Politecnico Di Milano), G. Maddinelli (Eni S.p.A.), A. Cominelli (Eni S.p.A.), A. Guadagnini (Politecnico Di Milano)

Summary

Water Alternating Gas (WAG) injection is one of the most successful enhanced oil recovery approaches. Properly accounting for the hysteretic effects of relative permeabilities is a critical issue encountered in numerical simulations of WAG at the mesoscale. Ranaee et al. (2015) proposed a sigmoid-based model for three-phase oil relative permeability, incorporating key physical effects taking place at the pore scale. The model can then be jointly used with the Larsen and Skauge (1998) model, accounting for gas relative permeability hysteresis, to develop a formulation for three-phase relative permeability suitable for reservoir simulation.

In this study we illustrate the impact of this joint formulation on a field scale setting through a suite of numerical simulations of WAG injection targeting a reservoir model inspired to real life cases. The analysis is performed by embedding the illustrated relative permeability models in the black oil model implemented in the Matlab Reservoir Simulation Toolbox (Lie et al., 2011). We assume non-hysteretic behavior for water relative permeability under water-wet conditions and characterize it upon relying on corresponding laboratory-scale data. As a baseline, the results are compared against a scenario in the absence of three-phase relative permeability hysteresis.

The computational domain is heterogeneous, the spatial distributions of porosity and absolute permeability varying across the ranges of [0.02 - 0.3] and [0.1 - 2600 mD], respectively. The model is set at equilibrium conditions, production being driven by three peripheral injectors and five up-dip producers. A given flow rate is assigned to each injector and a target value of liquid production rate is imposed at the producing wells. The numerically evaluated production rates constitute our target state variables. The schedule of the injectors is set to achieve a preliminary waterflooding phase followed by a WAG injection scheme. The latter is implemented by periodically switching the injected phase between water and gas for two injectors, the third injector continuously injecting water. The numerical simulations are performed through a fully implicit discretization of the equations governing the system dynamics. To minimize computational costs, we employ an algebraic multi-grid method and resort to a multi-processor high performance clustered computer system. Our results suggest that hysteretic effects are important across significant portions of the studied reservoir system. Field production responses are associated with a simultaneous increase of ultimate oil recovery and a corresponding decline of the gas-oil ratio when hysteretic effects are included in the simulations.

Introduction

Water-Alternating-Gas (WAG) injection is considered as a favorable tertiary oil recovery technique, with significant successful applications (Skauge et al., 2003). Similar to other flooding techniques, the performance of WAG depends on the macroscopic (volumetric) and microscopic (displacement) efficiency of the flooding process (Speight, 2009). Total oil recovery efficiency is then a result of a combination of displacement and volumetric efficiencies (Thakur and Satter, 1998). A WAG injection tends to combine high macroscopic sweep efficiency of the waterflooding operation with high displacement efficiency of the gas injection process to improve oil recovery (Kulkarni and Rao, 2005; Afzali et al., 2018).

In several cases, failures of EOR projects have been associated with the spatial heterogeneity of the reservoir properties. Birarda et al. (1990) observed that the gas phase tends to move to the high permeability regions and to bypass low permeability zones. Accordingly, gas fingering and early gas breakthrough may occur from fractures and high permeable layers. Otherwise, the water phase can also flow across lower permeability zones. Then, the combined use of water slugs along with gas injection can improve the overall sweeping efficiency.

Afzali et al. (2018) show that the flow rate in each region of the reservoir is proportional to the local flow capacity (i.e., the local conductivity). At high WAG ratios, gas tends to enter the highly permeable zones. Thus, highly permeable reservoir layers can be quickly filled and might contain compressed fluids in excess of their capacity during gas injection cycles. As water is injected, it sweeps the zones already occupied by gas and modifies the local mobility ratio.

Relative permeability is a key parameter that is typically assumed to imbue the impacts of heterogeneity, wettability, pore size distribution, Interfacial Tension (IFT), and fluid saturations. Caudle et al. (1951) were among the first to highlight the impact of hysteresis effects (hereinafter denoted as HEs) on the values of relative permeability of a non-wetting phase. Occurrence of such effects for the non-wetting and the intermediate wetting phases have been documented by a set of experimental (e.g., Oak, 1990; Alizadeh and Piri, 2014a; Moghadasi et al., 2016) and theoretical (e.g., Killough, 1976; Carlson, 1981; Larsen and Skauge, 1998; Blunt, 2000; Shahverdi and Sohrabi, 2013; Kianinejad et al., 2015; Ranaee et al., 2017, 2016) studies. The main reasons underpinning the lack of reversibility of the saturation paths observed under three-phase conditions are (*i*) trapping of the non-wetting phase during imbibition, (*ii*) remobilization of the intermediate phase through a layer drainage displacement mechanism, and (*iii*) wettability alteration (change) during drainage and imbibition (Piri and Blunt, 2005; Van Dijke et al., 2006; Suicmez et al., 2007; Sohrabi et al., 2008).

Hysteresis effects on water can be neglected under water-wet conditions. Otherwise, they should be captured when evaluating gas and oil relative permeabilities, as documented by experimental evidences (Oak et al., 1990; Di Carlo et al., 2000; Alizadeh and Piri, 2014b; Moghadasi et al., 2016) and theoretical analyses (Piri and Blunt, 2005; Spiteri and Juanes, 2006; Van Dijke et al., 2006; Bianchi Janetti et al., 2015). Some classical three-phase relative permeability models allow including HEs on gas relative permeability by updating model parameters at a given location in the reservoir according to the calculated changes of the saturation path. Skauge and Larsen (1994) designed a set of WAG injection experiments under differing rock wettability states and in the presence of unsteady state conditions. These authors estimated three-phase relative permeability at various stages of gas and water injection cycles. Hysteresis was shown to affect the relative permeability of the non-wetting (gas) phase to the largest extent. At a given saturation, relative permeability to the non-wetting phase was lower during the imbition cycle (i.e., when decreasing gas saturation) than during drainage cycles (i.e., when increasing gas saturation). Larsen and Skauge (1998) present a relative permeability model that takes into account HEs on the evaluation of gas relative permeability in a three-phase environment. The model also considers the reduced mobility and irreversible hysteresis loops that can take place during a three-phase flow of the kind associated with WAG injection processes. Egermann et al. (2000) suggested that hysteresis depends on saturation history and displacement history.

Accordingly, they considered two types of hysteresis, respectively termed as mechanism (imbibition/ drainage) and cycle (history) hysteresis. They also concluded that two-phase hysteresis models (e.g., Killough, 1976; Carlson, 1981) are not apt at adequately describing secondary and tertiary WAG processes. A review of the models that are commonly used to include HEs on gas relative permeability and their applicability in reservoir simulations is given by Hoseini et al. (2011).

Ranaee et al. (2015) develop a sigmoid-based model for the evaluation of HEs on three-phase oil relative permeability. Ranaee et al. (2016, 2017) assessed the applicability of such a formulation in comparision with a set of widely used (non-hysteretic) as well as recently developed (hysteretic) models in reproducing oil relative permeability data collected under coreflooding laboratory experiments.

Here, we consider numerical modeling of WAG injection at the mesoscale by including hysteretic effects of oil and gas three-phase relative permeabilities. We couple the sigmoid-based model proposed by Ranaee et al. (2015) for the evaluation of three-phase oil relative permeability with the Larsen and Skauge (1998) model, accounting for gas relative permeability hysteresis. The resulting formulation enables us to effectively include three-phase relative permeability hysteresis in reservoir simulation.

Methodology

We consider a black oil model, according to which simulation of three-phase fluid flow relies on the following set of equations (e.g., Chen et al., 2006)

$$\frac{\partial}{\partial t}\left(\frac{\phi S_\alpha}{B_\alpha}\right)+\nabla\cdot\left(\frac{\mathbf{v}_\alpha}{B_\alpha}\right)-\frac{q_{\alpha,s}}{B_\alpha}=0 \qquad \text{for} \qquad \alpha=w,o \tag{1}$$

$$\frac{\partial}{\partial t}\left[\phi\left(\frac{S_g}{B_g}+\frac{R_s S_o}{B_o}\right)\right]+\nabla.\left(\frac{\mathbf{v}_g}{B_g}+\frac{R_s\mathbf{v}_o}{B_o}\right)-\left(\frac{q_{g,s}}{B_g}+\frac{R_s q_{o,s}}{B_o}\right)=0 \tag{2}$$

$$\mathbf{v}_\alpha=-\frac{k_{r\alpha}\mathbf{k}}{\mu_\alpha}\left(\nabla p_\alpha-\rho_\alpha\wp\nabla z\right) \qquad \text{for} \qquad \alpha=w,o,g \tag{3}$$

Here, indices w, g and o respectively denote water, oil and gas phases; $\mathbf{k}$ [L^2] is the absolute permeability tensor; ϕ [-] is porosity; $\wp$ [LT^{-2}] is gravity; z [L] indicates a vertical coordinate; t [T] is time; R_s [-] is the dissolved gas-oil ratio; $q_{\alpha,s}$ [T^{-1}] is the source/sink term of fluid phase α evaluated at standard conditions; S_α [-], p_α [$MT^{-2}L^{-1}$], μ_α [$MT^{-1}L^{-1}$], ρ_α [ML^{-3}], $k_{r\alpha}$ [L^2], and $\mathbf{v}_\alpha$ [LT^{-1}] respectively denote saturation, pressure, viscosity, density, relative permeability and Darcy velocity of fluid phase α at reservoir conditions; B_α [-] is the formation volume factor. Density ρ_α in (3) is evaluated as

$$\rho_w=\frac{\rho_{w,s}}{B_w};\quad \rho_o=\frac{R_s\rho_{g,s}+\rho_{o,s}}{B_0};\quad \rho_g=\frac{\rho_{g,s}}{B_g} \tag{4}$$

Here, $\rho_{\alpha,s}$ is the density of the α-phase at standard conditions. Solution of equations (1)-(4) is subject to (*a*) considering the constraint $S_w+S_o+S_g=1$, (*b*) neglecting effects of capillary pressure, (*c*) imposed initial and boundary conditions, as well as (*d*) using a set of mathematical formulations conducive to evaluating three-phase relative permeabilities, $k_{r\alpha}$. Here, we assume the absence of HEs for three-phase water relative permeability (k_{rw}) under water-wet conditions. We then rely on the Larsen and Skauge (1998) model for the evaluation of gas (k_{rg}) relative permeability and of the formulation of Ranaee et al. (2015) for the evaluation of three-phase oil (k_{ro}) relative permeability.

According to the Larsen and Skauge (1998) formulation, gas relative permeability during imbibition, $k_{rg} = k_{rg}^{I}$, and drainage, $k_{rg} = k_{rg}^{D}$, are respectively evaluated as

$$k_{rg}^{I}(S_g) = \bar{k}_{rgo}^{d}(S_{gf}) \tag{5}$$

$$k_{rg}^{D}(S_g) = k_{rg}^{I}(S_{gi}) + (\bar{k}_{rgo}^{d}(S_g) - \bar{k}_{rgo}^{d}(S_{gi}))\left(\frac{\bar{S}_{wc}}{S_{wi}}\right)^{C_\alpha} \tag{6}$$

Here, C_α is the secondary drainage reduction coefficient, S_{gi} and S_{wi} respectively are gas and water saturations at the beginning of gas drainage, and S_{gf} is flowing gas saturation given by

$$S_{gf} = \bar{S}_{gc} + \frac{1}{2}\left\{S_g - S_{gt} + \sqrt{(S_g - S_{gt})\left(S_g - S_{gt} + \frac{4}{C_L}\right)}\right\} \tag{7}$$

where $\bar{S}_{gc}$ is the critical gas saturation obtained from gas-oil drainage data, C_L is the Land trapping coefficient, and S_{gt} is the trapped gas saturation for a three-phase system at the end of an imbibition process. The latter is computed as (Land, 1968)

$$S_{gt} = \bar{S}_{gc} + \frac{S_{gi} - \bar{S}_{gc}}{1 + C_L(S_{gi} - \bar{S}_{gc})} \qquad \text{with } C_L = \frac{1}{\bar{S}_{gt} - \bar{S}_{gc}} - \frac{1}{\bar{S}_{go}^{M} - \bar{S}_{gc}} \tag{8}$$

where $\bar{S}_{go}^{M}$ is the largest gas saturation observed in an oil-gas system at the end of gas injection; and $\bar{S}_{gt}$ is trapped gas at the end of oil injection.

Ranaee et al. (2015) introduced the following sigmoid-based (SB) model to capture HEs in the evaluation of three-phase oil relative permeability under waterflooding, $k_{ro} = k_{ro}^{W}$, and gas injection, $k_{ro} = k_{ro}^{G}$:

$$k_{ro}^{W} = \frac{(S_w - \bar{S}_{wc})k_{ro}^{S,W} + (S_g - \bar{S}_{gt})\bar{k}_{rog}^{d}}{(S_w - \bar{S}_{wc}) + (S_g - \bar{S}_{gt})}; \qquad k_{ro}^{G} = \min\left[\bar{k}_{row}^{d},\ \max(k_{ro}^{S,G}, \bar{k}_{rog}^{d})\right] \tag{9}$$

where $k_{ro}^{S,X}$ (with $X = G, W$) is given by

$$k_{ro}^{S,X} = \frac{\bar{k}_{row}^{M} S_o}{\bar{S}_{ow}^{M} + \exp\left[\theta_{1,X} - \theta_{2,X}\left(\frac{S_o}{\bar{S}_{ow}^{M}}\right)^{\bar{S}_{ow}^{M}}\right]} \tag{10}$$

Here, $\bar{k}_{row}^{M}$ is the value of $\bar{k}_{row}^{i}$ corresponding to oil saturation $\bar{S}_{ow}^{M} = 1 - \bar{S}_{wc}$. Model parameters $\theta_{1,X}$ and $\theta_{2,X}$ in (10) can be evaluated on the basis of two-phase data (oil-gas and oil-water) according to:

$$\begin{aligned}
\theta_{1,X} &= \ln\left[\frac{\bar{k}_{row}^{M} S_o^{inf,X}}{k_{ro}^{inf,X}} - \bar{S}_{ow}^{M}\right] + \theta_{2,X}\left(\frac{S_o^{inf,X}}{\bar{S}_{ow}^{M}}\right)^{\bar{S}_{ow}^{M}} \\
\theta_{2,X} &= \frac{1}{\bar{S}_{ow}^{M}}\left(\frac{m_{inf,X} S_o^{inf,X}}{k_{ro}^{inf,X}} - 1\right)\left(1 - \frac{\bar{S}_{ow}^{M} k_{ro}^{inf,X}}{\bar{k}_{row}^{M} S_o^{inf,X}}\right)^{-1}\left(\frac{S_o^{inf,X}}{\bar{S}_{ow}^{M}}\right)^{-\bar{S}_{ow}^{M}}
\end{aligned} \tag{11}$$

where:

$$S_o^{inf,G} = S_{oi}; \qquad S_o^{inf,W} = \bar{S}_{row} + \frac{\bar{S}_{ow}^{M} - \bar{S}_{row}}{2}; \qquad k_{ro}^{inf,G} = \bar{k}_{row}^{d}(S_o^{inf,G}); \qquad k_{ro}^{inf,W} = \bar{k}_{row}^{i}(S_o^{inf,W}) \tag{12}$$

$$m_{inf,G} = \left.\frac{\partial \bar{k}_{rog}^{d}}{\partial S_o}\right|_{\bar{S}_{wc}}; \quad m_{inf,W} = \left.\frac{\partial \bar{k}_{row}^{i}}{\partial S_o}\right|_{S_o^{inf}} \tag{13}$$

S_{oi} in (12) being initial oil saturation evaluated at the onset of the switches of saturation paths from waterflooding to gas injection conditions (all remaining symbols having already been defined).

Reservoir model

Our study aims at providing an analysis of the impact of HEs on oil and gas relative permeability at the scale of a complex heterogeneous reservoir model with multiple injection and production wells. We rely on black-oil reservoir model formulation (1)-(4) to describe fluid flow. The heterogeneous geological model of the reservoir is patterned after a field scale setting (whose location cannot be disclosed due to confidentiality reasons). For the implementation of the methodology described in the previous section, we rely on the open-source Matlab® toolkit, MRST (Lie, 2016). The latter provides an efficient test platform for the development and testing of new techniques of reservoir characterization and simulation (Lie et al., 2011). For practical reasons, results of this work are converted in field units. We implement our modelling setting in the MRST toolbox according to the steps described in the following.

The reservoir is discretized into 142×122×34 non uniform grid blocks. These are depicted in Figure 1a, which includes both active and inactive cells. The model has three injector (i.e. I1 - I3) and five production (i.e. P1 - P5) wells, as illustrated in Figure 1a. Wells are screened differently across layers 1 to 26 of the reservoir. The top of the reservoir is at a depth of 75423 ft and the average reservoir thickness is almost 550 ft (see Figure 1.b).

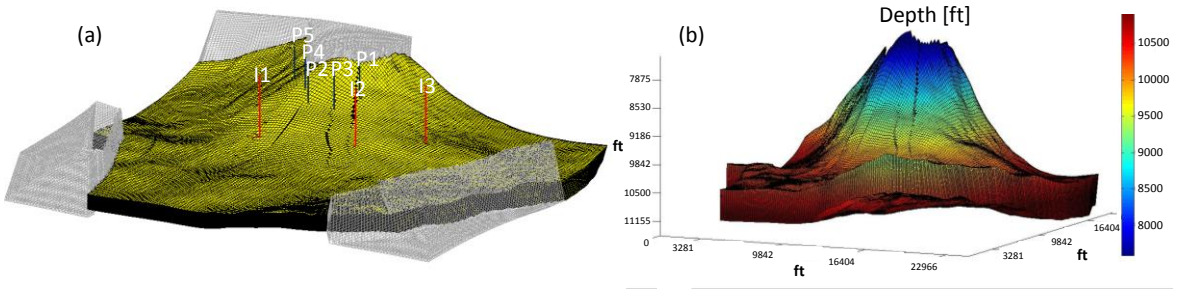

Figure 1 *geometry of the constructed reservoir model including (a) distribution of active and inactive computational cells and (b) depth of the cell centroids.*

Maps of the spatial distribution of absolute horizontal (i.e. k_x = k_y) and vertical (i.e. k_z) permeability and porosity values are depicted in Figure 2a-c. Average porosity and horizontal permeability are 0.187 and 766 mD, respectively. The model is structured according to three absolute permeability regions, each identified by a given permeability anisotropy ratio, respectively corresponding to k_z / k_x = 0.01, 0.10, and 0.40 (see Figure 2b).

Figure 2d depicts the spatial distribution of pore volume evaluated as $PV = ntgS_{oi}\phi V / B_{oi}$ rb, where *ntg* indicates the net-to-gross ratio and the distribution of initial oil saturation, S_{oi}, is evaluated from the initial reservoir state, as detailed in the following.

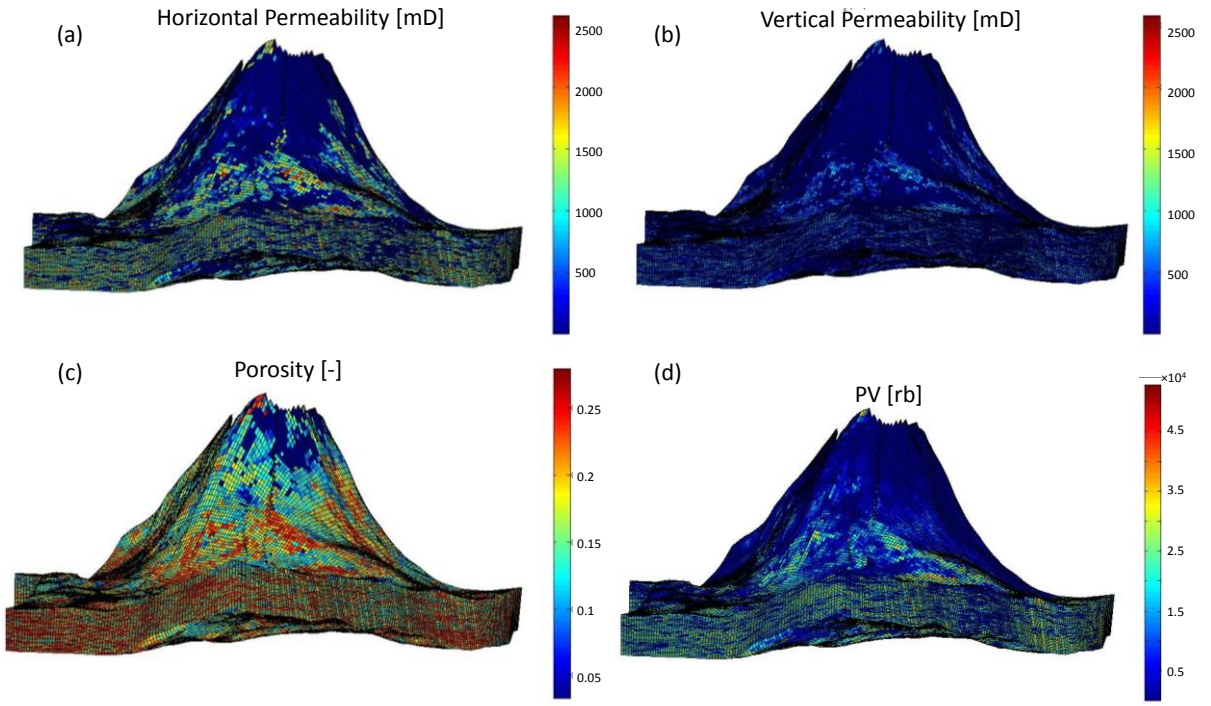

Figure 2 *spatial distribution of (a) horizontal permeability, (b) vertical permeability (c) porosity and (d) pore volume across the reservoir.*

In our study we assume the reservoir does not contain free gas initially. The saturation state of the reservoir at the onset of the flow simulations is set to the distribution of two-phase connate water saturation, i.e., $S_{oi} = 1 - \bar{S}_{wc}$, $S_{wi} = \bar{S}_{wc}$, $S_{gi} = 0$ for the computational cells locating above the water-oil contact (WOC) table, i.e. WOC = 9519.6 ft. The remaining portions of the simulation domain are initiated to be fully saturated by water (see Figure 3a). The initial pressure distribution (Figure 3b) is hydrostatic, with a reference pressure value p = 4248.3 psia at a reference depth of 9350.4 ft.

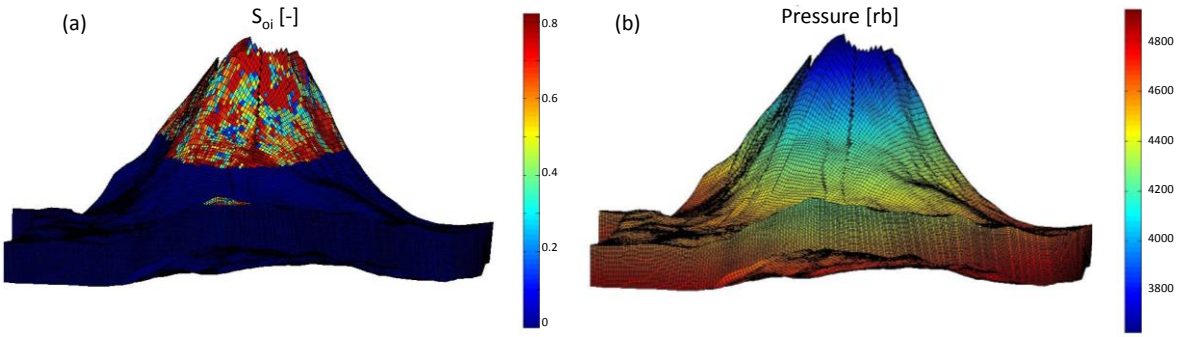

Figure 3 *(a) oil saturation and (b) pressure state conditions of the reservoir model at the onset of the simulations.*

Densities of water, oil and gas at standard conditions are set equal to 72.5, 53.7 and 60.89×10^{-3} lb/ft^3, respectively. Figure 4 depicts Pressure-Volume-Temperature (PVT) properties of the reservoir live oil and dry gas, in terms of pressure evolution of the formation volume factor of oil (B_o), and gas (B_g), PVT properties of water being set as:

$$B_w(p) = \frac{B_{w,ref}}{1 + C_w(p - P_{ref})(1 + C_w(p - P_{ref})/2)} \tag{14}$$

Here, $B_{w,ref}$ = 1.05 rb/stb, μ_w = 0.42 cP, and C_w = 2.12×10^{-6} 1/psi respectively are the formation volume factor, viscosity and compressibility of water at the reference pressure P_{ref} = 4248 psia.

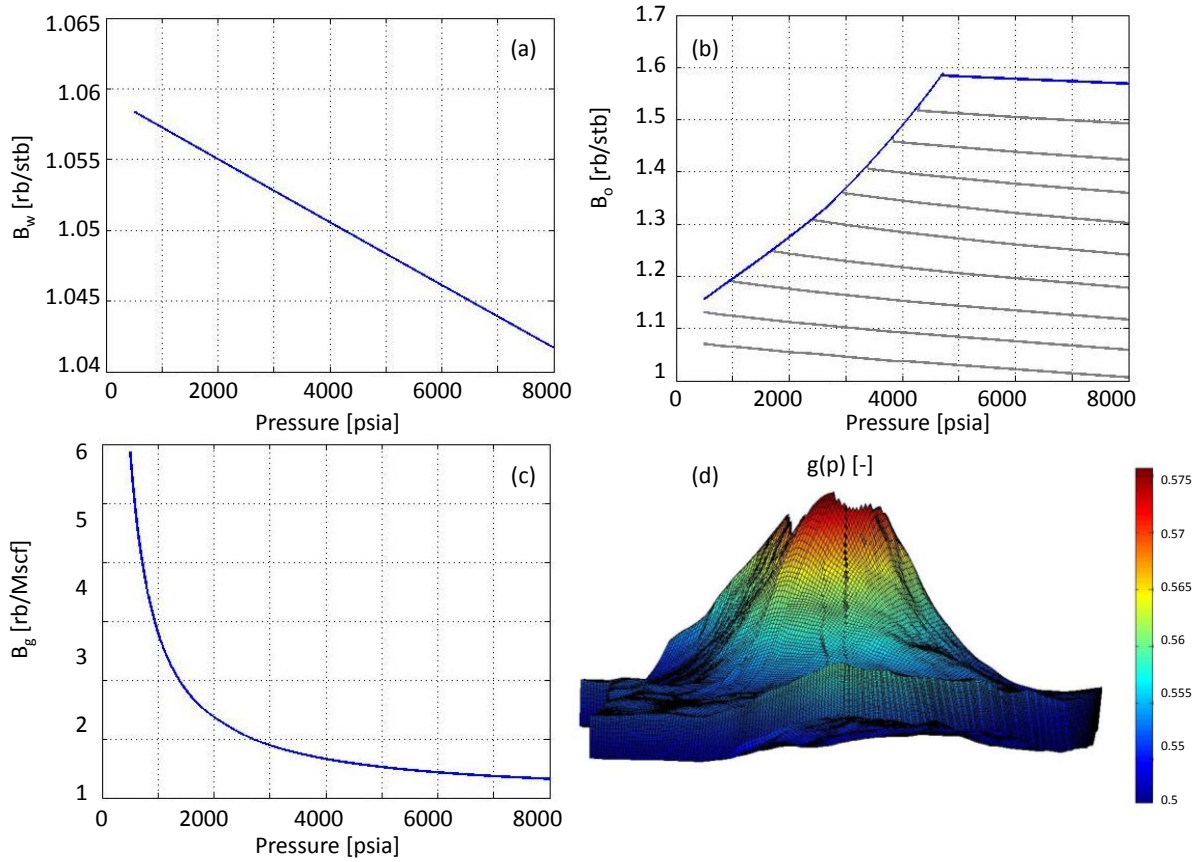

Figure 4 *Dependence of the formation volume factor of (a) water (B_w), (b) oil (B_o), and (c) gas (B_g) on pressure; (d) maximum fraction $g(\mathrm{p})$ of gas dissolved in the oil phase. Each grey curve in Figure 4b corresponds to a given bubble point pressure, identified through the intersection with the solid blue curve.*

It can be noted that even as one sets the initial state of a reservoir in the absence of free gas, there can be significant amounts of gas dissolved in the oil phase. Free gas can then appear when pressure drops below the bubble point pressure (see grey curves in Figure 4b). For a given pressure there is a fixed amount of gas that can be dissolved in the black-oil instantaneous dissolution model (Lie et al., 2011). Figure 4d depicts the function

$$g(\mathrm{p}) = \frac{R_s}{R_s^{sat}(\mathrm{p})} \tag{15}$$

where $g(\mathrm{p})$ represents the maximum fraction of gas dissolved in the oil phase considered in our simulations. A value $g(\mathrm{p}) \approx 1.0$ implies that the liquid is close to full saturation, so that free gas phase can then appear in the simulation model following pressure decrease (Lie et al., 2011). As one can see from Figure 4d, $0.5 \le g(\mathrm{p}) \le 0.6$ and free gas can appear during simulation.

Figure 5 depicts the way fluid viscosities depend on pressure. We can see that viscosity of the water phase (μ_w) does not depend on pressure, viscosity of the oil phase (μ_o) varying with pressure and dissolved gas.

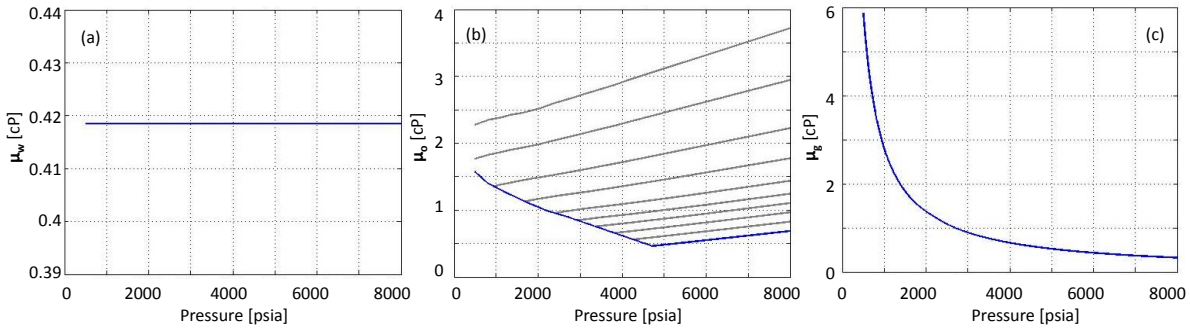

Figure 5 *Dependence of (a) water (μ_w), (b) oil (μ_o), and (c) gas (μ_g) viscosity on pressure. Each grey curve in Figure 5b corresponds to a given bubble point pressure, identified through the intersection with the solid blue curve.*

We define 6 regions of relative permeability across our computational domain (three drainage regions and three imbibition regions), as illustrated in Figure 6. Evaluation of three-phase relative permeabilities according to the formulation (5)-(13) relies on the availability of four sets of two-phase water (k_{rwo}), oil (in the presence of water, k_{row} , and gas, k_{rog}) and gas (k_{rgo}) relative permeability coreflooding data. Each of these may vary from drainage to imbibition conditions. We assign a given set of two-phase relative permeability curves to each of the drainage/imbibition regions identified in Figure 6. Figure 7 depicts the two-phase relative permeability curves we employ in our model.

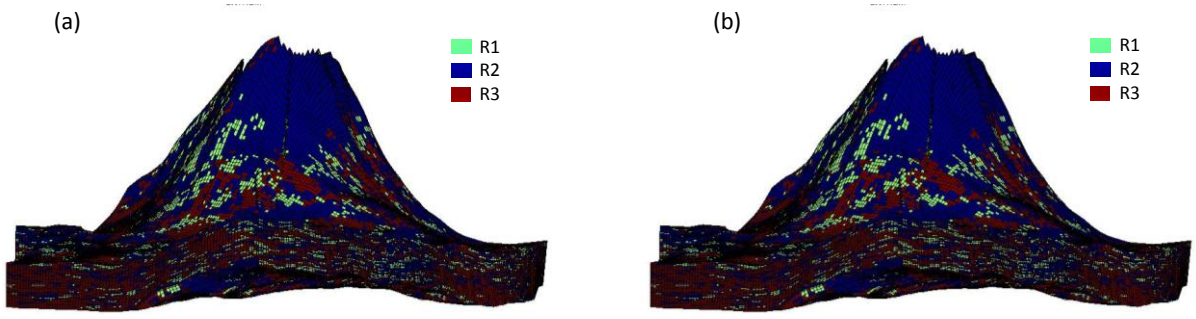

Figure 6 *Spatial distribution of the three (a) drainage and (b) imbibition regions. Regions are identified as Rj (j = 1, 2, 3).*

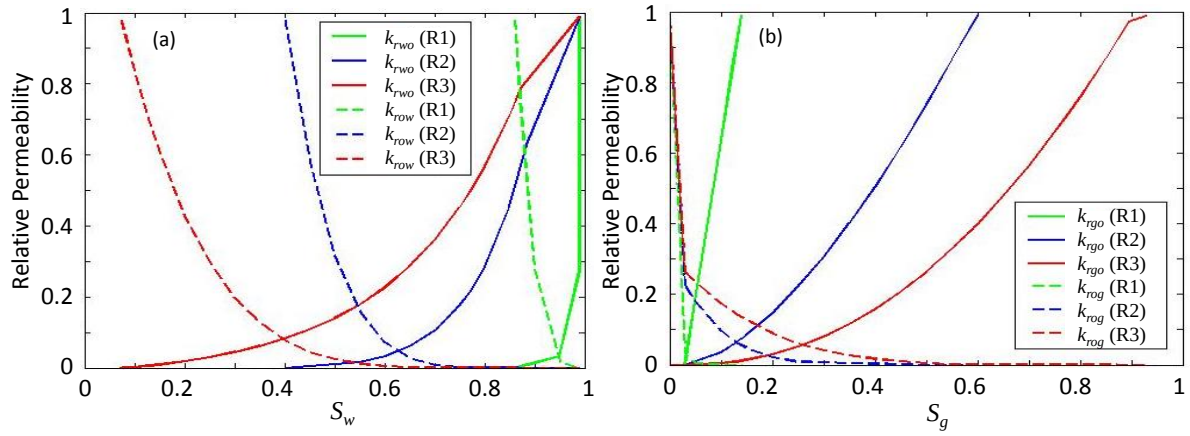

Figure 7 *Two-phase (a) water-oil and (b) gas-oil relative permeabilities assigned to the drainage/imbibition regions identified in Figure 6. Here, relative permeability curves are coded by colors corresponding to regions Rj (j = 1, 2, 3) identified in Figure 6.*

Evaluating two-phase relative permeability at a given computational cell relies on a standard technique (see Schlumberger Geo-Quest, 2010 for details) through which one rescales two-phase relative permeability curves assigned to each cell according to their saturation ending point values. Values of saturation ending points may vary between drainage/imbibition conditions. Figure 8 provides spatial distributions of connate water under drainage (SWCR) or imbibition (ISWCR), and critical (SGCR) or trapped (ISGCR) gas saturation ending points. We consider no rescaling for the residual oil saturations under drainage conditions. We also assume no hysteresis effects for the oil in the presence of gas phase, no rescaling being therefore implemented for two-phase residual oil saturation in the presence of gas under imbibition. When considering hysteresis effects for oil under imbibition condition (ISOWCR), we appropriately rescale $\bar{S}_{orw}$ values. Blunt (2000) argue that for a water-wet conditions the residual oil saturation in a two-phase oil-water imbibition setting is approximately equal to the total trapped hydrocarbon (oil and gas saturations) under gas-oil imbibition. Then, we assume that the oil saturation ending point in the presence of water under imbibition condition is higher than the corresponding value evaluated in the presence of gas.

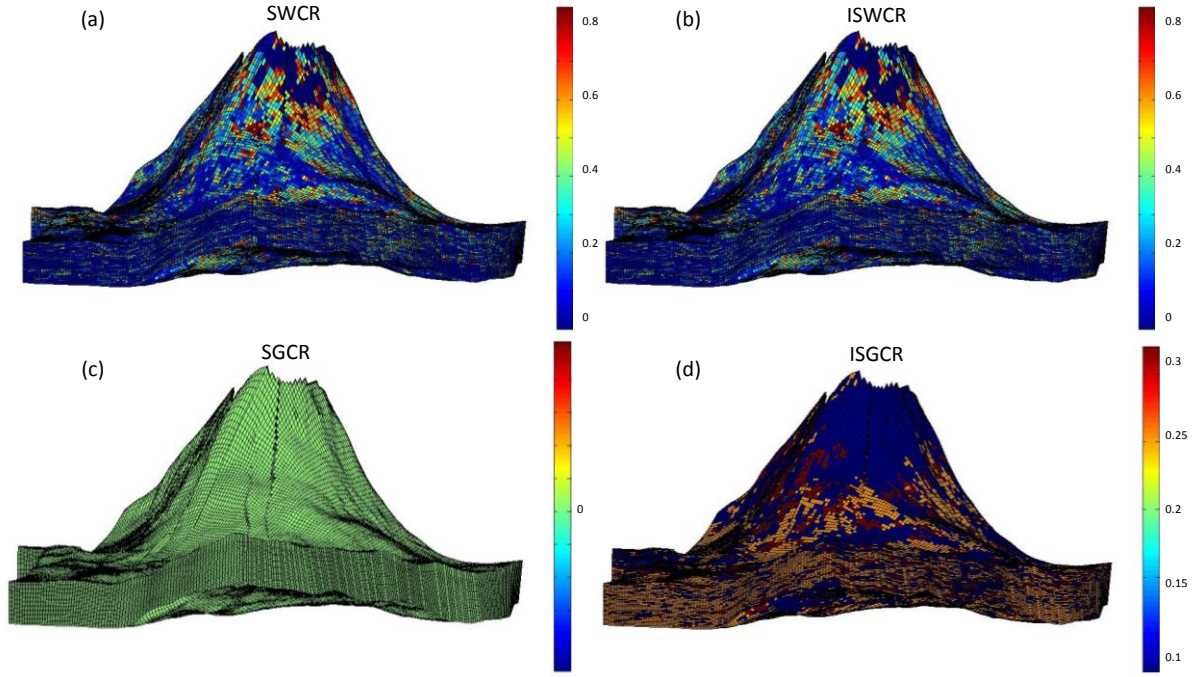

Figure 8 *Spatial distributions of connate water under drainage (SWCR) or imbibition (ISWCR), and critical (SGCR) or trapped (ISGCR) gas saturation ending points.*

We take advantage of non-uniform coarsening (NUC) tools (Hauge et al., 2012) available in MRST environment to amalgamate (grouping) cells from the fine numerical grid described above. We do so to prevent numerical convergence issues. Lie et al. (2017) show that if the permeability field displays strongly channelized features that separate high- and low-flow zones across the computational domain, numerical simulation may face convergence difficulties. An improved convergence of the numerical simulation may then be achieved by adapting the meshing of the reservoir model to the main features displayed by the permeability (or by the overall flow field).

Grouping of computational cells yields to a reduced complexity numerical model and is typically performed by: (*i*) grouping fine-grid numerical blocks which are as homogeneous as possible (in terms of permeability and/or flow); and (*ii*) tuning the resolution in areas of particular interest, i.e. high-flow regions. Accordingly, the NUC algorithm starts from a simulation cell and gradually forms a new block by adding neighboring cells. Aarnes et al. (2007) suggested to group cells according to

the logarithm of the velocity (or flux) magnitude, i.e. so that each coarse block is formed by a collection of cells having approximately the same magnitude of flow.

Figure 9a represents the results of our NUC implementation. The magnitude of velocity (in logarithmic scale) for a single phase (water) flow is used as cell-wise indicators guiding NUC. Figure 9b depicts the final reservoir model obtained.

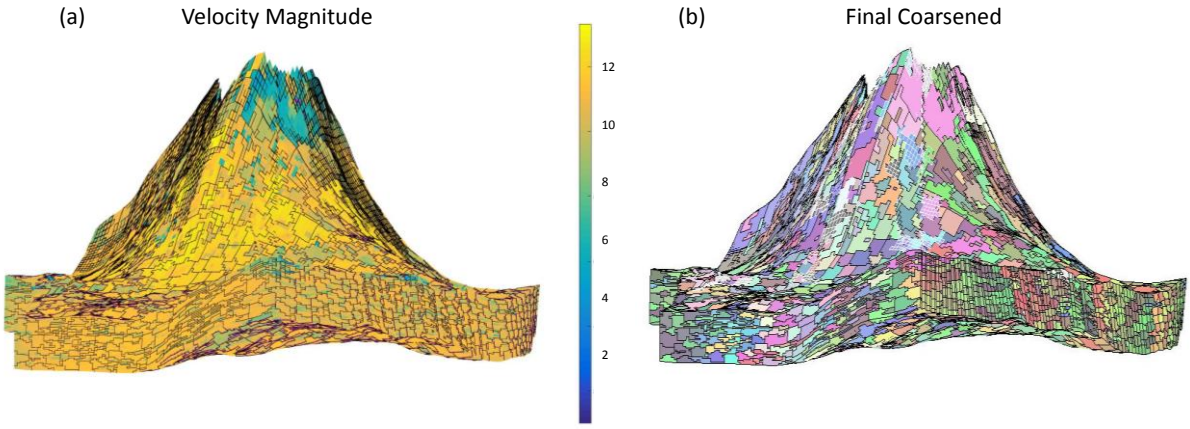

Figure 9 *Partitioning results following NUC implementation: (a) magnitude of the velocity (in logarithmic scale) for a single phase (water) flow considered as cell-wise indicators guiding NUC; (b) final coarsened reservoir model.*

In our study we rely on a constrained pressure residual, CPR-type, solver (Lie, 2016). The latter enables decoupling the fully implicit set of equations into a pressure and a transport component. Setting up a preconditioner improves the solution speed and is strictly required to solve our reservoir simulation problem. We then take advantage of an aggregation-based algebraic multigrid, AGMG, linear solver (see Notay, 2010; 2012; Napov and Notay, 2012 for details) to this end.

Key exemplary results

In the following we present the impact of HEs on some selected reservoir simulation outputs. We consider simulation scenarios where P1 - P5 production wells respectively operate at fixed liquid production rates of 15220, 4240, 5325, 5800 and 7700 stb/day while a lower bottom-hole-pressure (BHP) limit of 1700 psi is imposed to all producers. Injector I3 is set to waterflooding (with 10000 stb/day) during whole simulation time. We alternate gas injection and waterflooding at injectors I1 and I2 on an annual basis up to a total production life t_{LC} = 15 years. Injected flow rates at I1 and I2 are set at 20000 stb/day during waterflooding and at 20000 Mscf/day during gas injection. Note that I2 is injecting gas when I1 is set for waterflooding and vice versa. An upper BHP of 6000 psi is imposed to the injectors.

To include HEs in the evaluation of relative permeabilities, we extend the MRST toolbox and consider HEs on both the non-wetting and intermediate wetting phases through formulations (5)-(13). During reservoir simulation, we evaluate and update relative permeability values at each of the numerical blocks forming the system according to their saturation history (Ranaee et al., 2018), available two-phase relative permeability data are shown in Figure 7 and distribution of saturation ending points are provided in Figure 8. Results from non-hysteresis saturation-weighted interpolation three-phase relative permeability model (Baker, 1988) are also depicted for comparing purposes.

Figure 10 depicts field water cut (FWCT), oil recovery efficiency (FOE) and gas-oil ratio (FGOR) versus time. As expected, both modeling strategies (i.e. considering or neglecting hysteresis effects, respectively denoted as HYS and no-HYS in Figure 10) provide a similar trend before water breakthrough (t < 3 years), FWCT and FGOR (mildly) decreasing following WAG implementation. In

this setting, we further note that inclusion of HEs in the modeling workflow yields results suggesting that WAG is effective in increasing FOE with respect to results suggested by the No-HYS model at late production times.

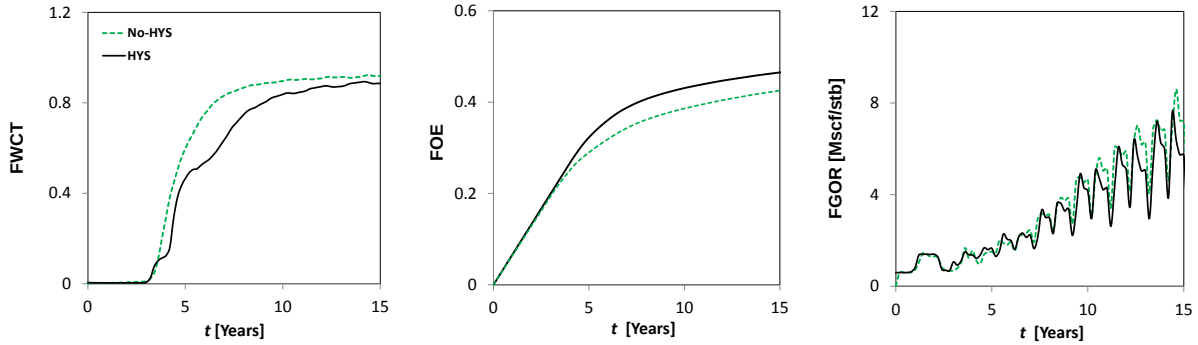

Figure 10 *Temporal evolution of (a) FWCT, (b) FOE and (c) FGOR across our simulation window when three-phase relative permeabilities are evaluated via non-hysteresis (No-HYS) and hysteresis (HYS) models.*

Conclusions

We study the impact of explicitly including HEs for relative permeabilities in numerical simulations of enhanced oil recovery approaches grounded on the application of WAG injection protocols. The analysis is performed in the context of scenarios implemented in a complex heterogeneous domain. Hysteresis Effects on non- and intermediate-wetting phases are considered by implementing the sigmoid-based model developed by Ranaee et al. (2015) for the oil phase and the Larsen and Skauge (1998) model for the gas phase. Effects of this modeling choice are assessed through comparison against a base case where neglecting hysteresis effects. Our study shows that inclusion of HEs in the numerical model typically yields an increased ultimate oil recovery and a mild decrease of gas-oil ratio and water cut, as compared to neglecting them.

Acknowledgments

This work was partially supported by a grant provided by Eni S.p.A. “Modellazione alla microscala e parametri effettivi per tecniche WAG”. *SINTEF Applied Mathematics* is acknowledged for allowing the use of MRST for research purposes.

References

Aarnes, J. E., Hauge, V. L., and Efendiev, Y. [2007] Coarsening of three-dimensional structured and unstructured grids for subsurface flow. *Adv. Water Resour.*, **30**(11), 2177-2193. doi: 10.1016/j.advwatres.2007.04.007.

Afzali S., Rezaei, N., and Zendehboudi, S. [2018] A comprehensive review on enhanced oil recovery by water alternating gas (WAG) injection. *Fuel*, **227**, 218-245.

Alizadeh, A.H. and Piri, M. [2014a] Three-phase flow in porous media: A review of experimental studies on relative permeability. *Rev. Geophys*. **52**(3), 468-521. doi:10.1002/2013RG000433

Alizadeh, A. H. and Piri, M. [2014b] The effect of saturation history on three-phase relative permeability: An experimental study. *Water Resour. Res.*, **50**(2), 1636-1664. doi:10.1002/2013WR014914

Bianchi Janetti, E., Riva, M. and Guadagnini, A. [2015] Analytical expressions for three-phase generalized relative permeabilities in water- and oil-wet capillary tubes. *Comput. Geosci.*, **20**(3), 555-565, doi:10.1007/s10596-015-9508-5

Birarda G.S. Dilger C.W. McIntosh I. [1990] Re-evaluation of the miscible WAG flood in the Caroline Field, Alberta. *SPE Reservoir Eng.*, **5**(4), 453-8.

Blunt, M.J. [2000] An empirical model for three-phase relative permeability. *SPE J.*, **5**(3), 435-445. SPE-56474-MS. doi:10.2118/67950-PA

Carlson, F.M. [1981] Simulation of relative permeability hysteresis to the nonwetting phase, SPE-10157-MS, Presented at the SPE Annual Technical Conference and Exhibition, San Antonio, Texas, USA, October 5-7. doi:10.2118/10157-MS

Caudle, B.H., Slobod, R.L. and Brownscombe, E.R. [1951] Further developments in the laboratory determination of relative permeability. *J. Petrol. Tech.*, **3**(5), 145-150. doi:10.2118/951145-G

Chen, Z., Huan, G., and Ma, Y. [2006] *Computational methods for multiphase flows in porous media*. SIAM Comp. Sci. Eng., Philadelphia. doi:10.1137/1.9780898718942

Di Carlo, D.A., Sahni, A. and Blunt, M.J. [2000] The effect of wettability on three-phase relative permeability, *Transp. Porous Med.*, **39**(3), 347-366. doi:10.1023/A:1006653323374

Egermann, P., Vizika, O., Dallet, L., Requin, C. and Sonier, F. [2000] Hysteresis in three-phase flow: experiments, modeling and reservoir simulations, SPE-65127-MS, Presented at the SPE European Petroleum Conference, Paris, France, 24-25 October. doi:10.2118/65127-MS

Hoseini, J., Masoudi, R., Mirkalaei, M., Mousa, S., Ataei, A. and Demiral, B. [2011] Investigating the effects of hysteresis modeling on numerical simulation of immiscible WAG injection, IPTC-15055-MS, Presented at the International Petroleum Technology Conference, Bangkok, Thailand, February 7-9. doi:10.2523/IPTC-15055-MS

Hauge, V.L. Lie, K.A. and Natvig, J.R. [2012] Flow-based coarsening for multiscale simulation of transport in porous media. *Comput. Geosci.* **16**(2), 391-408. doi: 10.1007/s10596-011-9230-x.

Kianinejad, A., Chen, X. *and* Di Carlo, D. A. [2015] The effect of saturation path on three-phase relative permeability, *Water Resour. Res.* **51**(11), 9141-9164. doi:10.1002/2015WR017185

Kulkarni, M.M. and Rao, D.N. [2005] Experimental investigation of miscible and immiscible water-alternating-gas (WAG) process performance. *J. Petrol. Sci. Eng.*, **48**(1), 1-20.

Killough, J. E. [1976] Reservoir simulation with history-dependent saturation functions. *SPE J.*, **16**(1), 37-48. SPE-5106-PA. doi:10.2118/5106-PA

Land, C.S. [1968] Calculation of imbibition relative permeability for two- and three-phase flow from rock properties. *SPE J.*, **8**(2), 149-156, SPE-1942-PA. doi:10.2118/1942-PA

Larsen, J.A. and Skauge, A. [1998] Methodology for numerical simulation with cycle-dependent relative permeabilities. *SPE J.*, **3**(2), 163-173. SPE-38456-PA. doi:10.2118/38456-PA

Lie, K.A. Kedia, K. Skaflestad, B. Wang, X. Yang, Y. Wu, X.-H. and Hoda, N. [2017] A general non-uniform coarsening and upscaling framework for reduced-order modeling, SPE-182681-MS, Presented at SPE Reservoir Simulation Conference, 20-22 February, Montgomery, Texas, USA. doi:10.2118/182681-MS

Lie, K.A. [2016] An introduction to reservoir simulation using MATLAB: user guide for the Matlab Reservoir Simulation Toolbox (MRST). https://www.sintef.no/projectweb/mrst/publications

Lie, K.A. Krogstad, S. Ligaarden, I.S. Natvig, J.R. Nilsen, H.M. and Skaflestad, B. [2011] Open source MATLAB implementation of consistent discretisations on complex grids. *Comput. Geosci.*, **16**(2), 297-322. doi:10.1007/s10596-011-9244-4.

Moghadasi, L., Guadagnini, A., Inzoli, F., Bartosek, M. and Renna, D. [2016] Characterization of two- and three-phase relative permeability of water-wet porous media through X-Ray saturation measurements, *J. Petrol. Sci. Eng.*, **145**, 453-463. doi:10.1016/j.petrol.2016.05.031

Napov A. and Notay, Y. [2012] An algebraic multigrid method with guaranteed convergence rate, *SIAM J. Sci. Comput.*, **34**, A1079-A1109. doi: 10.1137/100818509

Notay, Y. [2012] Aggregation-based algebraic multigrid for convection-diffusion equations, *SIAM J. Sci. Comput.*, **34**, A2288-A2316. doi:10.1137/110835347

Notay, Y. [2010] An aggregation-based algebraic multigrid method, *Electronic Transactions on Numerical Analysis*, **37**, 123-146.

Oak, M.J., Baker, L.E., and Thomas, D.C. [1990] Three-phase Relative Permeability of Berea sandstone. *J. Pet. Tech.*, **42**, 1054-1061.

Oak, M.J. [1990] Three-phase Relative Permeability of Water-wet Berea, SPE-20183-MS, Presented at 7th SPE/DOE Enhanced Oil Recovery Symposium, Tulsa, Oklahoma, April 22-25.

Piri, M. and Blunt, M. J. [2005] Three-dimensional mixed-wet random pore-scale network modeling of two and three-phase flow in porous media, I. model description. *Phys. Rev. E.*, **71**, 206-301. doi:10.1103/PhysRevE.71.026301

Ranaee, E., Inzoli, F., Riva, M. Cominelli, A. and Guadagnini, A. [2018] Propagation to reservoir simulation of uncertainty associated with three-phase relative permeability models with hysteresis, SPE-190825-MS, Presented at SPE Europec featured at 80th EAGE Conference and Exhibition, 11-14 June, Copenhagen, Denmark. doi:10.2118/190825-MS

Ranaee, E., Moghadasi, L., Inzoli, F., Riva, M. and Guadagnini, A. [2017] Identifiability of parameters of three-phase oil relative permeability models under simultaneous water and gas (SWAG) injection. *J. Petrol. Sci. Eng.* **159**, 942-951. doi: /10.1016/j.petrol.2017.09.062

Ranaee, E., Riva, M., Porta, G. M. and Guadagnini, A. [2016] Comparative assessment of three-phase oil relative permeability models. *Water Resour. Res.*, **52**(7), 5341-5356. doi:10.1002/2016WR018872

Ranaee, E., Porta, G. M., Riva, M., Blunt, M. J. and Guadagnini, A. [2015] Prediction of three-phase oil relative permeability through a sigmoid-based model. *J. Petrol. Sci. Eng.*, **126**, 190-200. doi:10.1016/j.petrol.2014.11.034.

Schlumberger Geo-Quest. 2010. ECLIPSE 100 Reference Manual.

Shahverdi, H. and Sohrabi, M. 2013. An improved three-phase relative permeability and hysteresis model for the simulation of a water-alternating-gas injection. *SPE J.*, **18**(5), 841-850. SPE-152218-PA. doi:10.2118/152218-PA

Skauge, A. and Stensen, J.Å. [2003] Review of WAG field experience, presented in first international conference and exhibition, modern challenges in oil recovery, Gubkin University, Moscow, Russia, 19-23 May.

Skauge, A, and Larsen, J.A. [1994] Three-phase relative permeabilities and trapped gas measurements related to WAG processes, Proceedings of the International Symposium of the Society of Core Analysts, Stavanger, Norway.

Sohrabi, M., Danesh, A. and Jamiolahmady, M. [2008] Visualization of residual oil recovery by near-miscible gas and SWAG injection using high-pressure micromodels. *Transp. Porous Med.*, **74**(2), 239-257. doi:10.1007/s11242-007-9193-5

Speight JG. [2009] *Enhanced recovery methods for heavy oil and tar sands*. Elsevier.

Spiteri, E. J. and Juanes, R. [2006] Impact of relative permeability hysteresis on the numerical simulation of WAG injection. *J. Petrol. Sci. Eng.*, **50**(2), 115-139. doi:10.1016/j.petrol.2005.09.004

Suicmez, V. S., M. Piri and Blunt, M. J. [2007] Pore-scale simulation of water alternate gas injection. *Transp. Porous Med.*, **66**(3), 259-286. doi:10.1007/s11242-006-0017-9

Thakur, G.C. and Satter, A. [1998] *Integrated waterflood asset management*. PennWell Books.

Van Dijke, M. I. J., Sorbie, K. S. Sohrabi, M. and Danesh, A. [2006] Simulation of WAG floods in an oil-wet micromodel using a 2-D pore-scale network model. *J. Petrol. Sci. Eng.*, **52**: 71-86. doi:10.1016/j.petrol.2006.03.014